Journal of Materials Chemistry A

Accepted Manuscript

ROYAL SOCIETY OF CHEMISTRY

www.rsc.org/materialsA

Journal of Materials Chemistry A

ARTICLE

Catalytic activity of polymerized self-assembled artificial enzyme nanoparticles: applications to microfluidic channel-glucose biofuel cell and sensor†

Hui-Bog Noh and Yoon-Bo Shim*

Synthesized catalysts composed of hydrazine-bearing conducting polymer nanoparticles (poly[2,2′:5′,2′′-terthiophene-3′-yl hydrazine] (polyTHyd) and (poly[4-([2,2′:5′,2′′-terthiophen]-3′-yl) phenyl) hydrazine] (polyTPHyd)) were prepared through self-assembling of monomers on gold nanoparticles (monomers-AuNPs: dia. 7.5 ± 2.0 nm). The monomers self-assembled on AuNPs were electrochemically polymerized to form conducting polymer nanoparticles, which possessed an enzyme-like catalytic activity for the reduction of H_2O_2. The polymer-assembled nanoparticles immobilized on the microfluidic channel electrodes revealed well defined direct electron transfer (DET) processes, which were observed at +54.5/-20.9 and +64.8/+3.6 mV for polyTHyd and polyTPHyd. Glucose oxidase (GOx) and horseradish peroxidase (HRP) were immobilized on the carboxylated polyterthiophene (poly[2,2′:5′,2″-terthiophene-3′-(p-benzoic acid)])-assembled nanoparticle layer to use as counter electrodes in the cells. The performance of microfluidic biofuel cells composed of a GOx-modified anode and cathodes of HRP and hydrazine-bearing polymer-assembled nanoparticles were compared with using a standard glucose, urine, and whole blood samples as fuels. The cell operated with a 10.0 mM glucose solution generated a maximum electrical power density of 0.78 ± 0.034 mW cm^{-2} and an open-circuit voltage of 0.48 ± 0.035 V. The cell was also examined as a glucose-sensing device, which had a dynamic range of 10.0 μM - 5.0 mM with a detection limit of 2.5 ± 0.2 μM under alternating current potential modulation.

Received 00th January 20xx,
Accepted 00th January 20xx

DOI: 10.1039/x0xx00000x

www.rsc.org/

Introduction

Numerous studies for biofuel cells (BFCs) using microbial and enzymes have been performed since the first demonstration of microbial fuel cells in 1911.[1-3] Of these, microbial fuel cells employing whole live cells have a longer lifetime[4] and higher energy density than enzymatic fuel cells. Although enzymatic fuel cells have some disadvantages, considerable attention has also been paid to their development because of the ambient working conditions, neutral working pH, and, more importantly, the possibility of using them *in vivo* for power production[5-7] and for implantable biosensors to monitor biological target molecules (*e.g.*, glucose).[6,8,9] Hence, the study of enzymatic BFCs must be directed to expand the effective cell lifetime and power density through a new advanced catalyst immobilization. One important step to expand the performance and lifetime of enzyme-based BFCs is to attain a stable electrode surface for the fixation of enzymes or catalytic materials.[5,10] One of ways to enhance the stability and the performance of catalytic electrodes is to form of stable and active catalytic nanoparticle layer on the electrode surface,[11-14] where the thickness of the layer is a few nanometers or less, allowing it to easily shuttle electrons between the electrode surface and the active sites of the fixed enzymes or enzyme-like catalytic materials.

Thus, it is crucial to study a method forming stable and active catalytic nanoparticle layers that allow the fast electron transfer. One of the ways to obtain a highly stable electrode surface is the use of conductive polymer layer-assembled nanoparticles to carry artificial enzymes. Although improvements in the bioactivity and the power density of enzymatic fuel cells have been achieved through use of metallic polymers, mediators, and cofactors, there have been limited improvements in stability, so far.[15,16] Hence, it is possible to enhance the cell performance by constructing a highly stable and facile probe surface using nanotechnology. This construction may be achieved through the chemical binding of enzymes or synthetic catalyst nanoparticles on a stable electrical conductive polymer, which bears various functional groups, such as -COOH, -NH_2, benzoic acid, and others.[17-19]

The BFCs and biosensors using stable conductive polymers exhibit unique properties, including high stability over a wide range of pH values, thermal stability, and exceptional resistance to other chemicals.[20-23] Moreover, some π-conjugated polymers stabilize redox enzymes and proteins because the polymer possess reducing and oxidizing capabilities that allow it to act as a redox buffer,[11,24,25] which may protect the deactivation of the enzyme and redox proteins. To achieve an improved performance in BFCs as well as

[a] Department of Chemistry and Institute of Biophysio Sensor Technology (IBST), Pusan National University, Busan 609-735, Republic of Korea.
E-mail: ybshim@pusan.ac.kr

† Electronic Supplementary Information (ESI) available: Additional Preparation of AuNPs, fabrication of the screen-printed microchannel electrode (SPME) (Fig. S1), performance of the MBFCs (Table S1), and comparison of the electrical outputs for BFCs (Table S2). See DOI: 10.1039/x0xx00000x

the stability, the electro-catalytic activity of the electrode material in the nanostructure is also important. Thus, we attempted to synthesize catalytic electrode materials based on stable polyterthiophene analogs bearing a hydrazine group as an enzyme-like catalyst that enhanced the electrochemical catalytic activity for the reduction of H_2O_2.

The efficiency of a BFC can be enhanced by increasing the active surface to the volume ratio, which can be achieved through the use of a microfluidic channel.[26-29] The microfluidic channel biofuel cell (MBFC) offers several key advantages, such as increased rates of mass transfer, low amounts of reagents, increased safety using smaller volumes, and coupling of different microsystems.[30-32] It is also possible to create the compartmentalization of the oxidant and the glucose fuel streams in a single channel without any physical barrier while still allowing ionic transport.[33-35] Thus, we attempted to assemble a microfluidic channel BFC in which biocatalysts can be easily immobilized on the channel wall using carbon electrode materials. In addition, the microfluidic channel immobilized with catalytic nanoparticles can be used for flexible biosensor devices including a flexible MBFC to finally implant it into animal body and to apply for a wearable device.

In the present study, we synthesized monomer precursors of π-conjugated conducting polymers bearing a catalyst group as a synthetic enzyme. We compared the catalytic property between hydrazine-bearing conducting polymer nanoparticles formed electrochemically with monomers assembled on AuNPs and an enzyme-modified layer. The HRP/polyTBA-AuNP, polyTHyd-AuNP, and polyTPHyd-AuNP electrodes were used as cathodes and GOx fixed on a polyTBA-AuNP as an anode. Each surface of self-assembled nanoparticles was characterized by UV-visible spectroscopy, transmission electron microscopy (TEM), atomic force microscopy (AFM), quartz crystal microbalance (QCM), and cyclic voltammetry (CV). The efficiency of the DETs process for enzymes and synthesized polymer catalysts was examined, and screen-printed microfluidic channel BFCs made of carbon channel electrodes were constructed to demonstrate their cell and biosensor performance.

Experimental

Material and Reagents

Glucose oxidase (GOx) (EC 1.1.3.4, 166 units/mg, molecular weight: approx. 153,000 Da) and horseradish peroxidase (HRP) (EC 1.11.1.7, 128 units/mg, molecular weight: approx. 40,000 Da) were purchased from Toyobo Co. (Japan) and stored as received at -20 °C. D-(+)-Glucose, 1-ethyl-3-(3-dimethylaminopropyl) carbodiimide (EDC), *N*-hydroxysuccinimide (NHS), $HAuClO_4 \cdot 3H_2O$ (≥99.9%), HCl (37%), trisodium citrate, sodium borohydride, acetonitrile, di(propylene glycol) methyl ether, and tri(propylene glycol) methyl ether were purchased from Sigma-Aldrich Co. (USA) and were used as received. Tetrabutylammonium perchlorate (TBAP, electrochemical grade) was purchased from Fluka (USA) and purified according to a general method, followed by vacuum drying at 1.33×10^{-3} Pa.[19] N_2 gases were used as received from P. S. Chem (S. Korea). A terthiophene monomer, 2,2′:5′,2″-terthiophene-3′-(*p*-benzoic acid) (TBA), was synthesized using a previously reported method,[36] and THyd and TPHyd were newly synthesized. PBS (pH 7.0) was prepared by mixing sodium dihydrogen phosphate with disodium hydrogen phosphate (Sigma-Aldrich Co., USA). All aqueous solutions were prepared in double distilled water, which was obtained from a Milli-Q water purifying system (18 MΩ cm). All other chemicals were of extra-pure grade.

Instruments

CVs were recorded by using a potentiostat/galvanostat, Kosentech model KST-P2 (S. Korea). A Bruker Avance 300 Spectrometer (Germany) was used to record the ^{1}H- and ^{13}C-NMR spectra in $CDCl_3$. The FT-IR spectrum was obtained with a JASCO FT-IR spectrometer (UK). The molecular weight of the synthesized compounds was determined with a JEOL JMS-700 mass spectrometer (MS) (Japan). The microfluidic channel was visualized using a microscope (SOMETECH Model MV-324, S. Korea). UV-visible spectra were obtained with a UV-3101PC, Shimadzu (Japan). A JEOL JEM-2010 electron microscope (Jeol High-Tech. Co., Japan) with an acceleration voltage of 200 kV was used to record TEM images. AFM images were captured under ambient conditions by using a Multimode AFM device (Veeco Metrology) equipped with a Nanoscope IV controller (Veeco). QCM experiments were performed by using a SEIKO EG&G model QCA 917 and a PAR model 263A potentiostat/galvanostat (USA). A Au-coated working electrode (area: 0.196 cm^2; 9.0 MHz; ATcut quartz crystal) was used for the QCM experiments. The voltage and current generated by the MBFCs were measured by applying an external variable load resistance (Eddidatek Co. model RU-610, S. Korea) and by using a digital multi-meter (Taekwang Industrial Co. model TK-4002, S. Korea). A function generator (GSI, Model Protek 9340, S. Korea) was used to apply an alternating current (AC) electric field to the microchannel electrode within the MBFC.

Synthesis of Terthiophene Monomers

Synthesis of 2,2′:5′,2″-terthiophene-3′-(*p*-benzoic acid) (TBA)

TBA was synthesized by the following procedure: 3′-bromo-5,2′-5′,2″-terthiophene (BTT) (compound (**1**)) was treated with *n*-BuLi and trimethyl borate in Et_2O under an N_2 atmosphere at -83 °C to yield 5,2′:5′,2″-terthiophene-3′-boronic acid (TTB). The Suzuki coupling of TTB with 4-bromobenzonitrile in a refluxing two-phase solution of toluene/water (5:1) in the presence of $NaHCO_3$ and $Pd(PPh_3)_4$ formed 3′-(4-benzonitrile)-2,2′-5′,2″-terthiophene (BNTT). BNTT and KOH and a refluxing mixture solution of ethoxyethanol/water (5:1) yielded TBA. The detailed synthesis procedure and characterizations have been previously described.[36]

Synthesis of 2,2′:5′,2″-terthiophene-3′-yl hydrazine (THyd) (compound (2))

A typical preparation of (**2**) began with BTT (**1**) (2.0 g, 6.1 mmol) and 1.5 mL of 80% hydrazine hydrate in 20.0 mL of methoxy ethanol heated under reflux for 5 h. After the mixture cooled to room temperature, the precipitated product was filtered, washed with ethanol, and dried to give 1.13 g of a yellow solid with a yield of 67%. The characteristics were as follows: mp 118 °C; IR (KBr): 3405 - 3509 (br s), 2983, 2873, and 2834 cm^{-1}; ^{1}H NMR ($CDCl_3$) δ: 7.45 (dd, *J* = 1.6, 4.8 Hz, 1H), 7.37 (dd, *J* = 1.5, 6.2 Hz, 1H), 7.28 (dd, *J* = 1.5, 6.2 Hz, 1H), 7.19 (dd, *J* = 1.5, 4.5 Hz, 1H), 7.09 - 7.12 (m, 2H), 7.05 (dd, *J* = 4.9, 6.1 Hz, 1H), 5.19 (br s, 1H), and 3.57 (br s, 2H); ^{13}C NMR ($CDCl_3$): 139.1, 136.6, 134.1, 130.6, 129.1, 127.7, 127.1, 126.6, 126.2, 125.3, 124.8, and 110.7; Anal $C_{12}H_{10}N_2S_3$; MS (EI) *m/z* (%): 278 (M+, 53), 263 (31), 247 (100), 195 (32), 165 (28), and 83 (74).

Synthesis of 4-([2, 2':5', 2''-terthiophen]-3'-yl) aniline (TTPA) (compound (4))

A degassed diethyl ether solution (15.0 mL) of BTT (3.27 g, 10.0 mmol), which was prepared from thiophene, was slowly reacted with tetramethylethylenediamine (TMEDA) (1.8 mL, 12.0 mmol) and 1.6 M *n*-BuLi (7.5 mL, 12.0 mmol) at -83 °C under a N_2 atmosphere. The reaction mixture was stirred for 1 h at -83 °C, and trimethyl borate (2.2 mL, 20.0 mmol) diluted in diethyl ether (30.0 mL) was added. The mixture was allowed to warm to room temperature and was stirred for 4 h, after which 2.0 M HCl (20.0 mL) was added. After 1.5 h of additional stirring, crude TTB (compound (**3**)) precipitated out as a white solid, which was washed with water and dried under reduced pressure. The crude TTB, $NaHCO_3$ (8.40 g), 4-bromoaniline (2.06 g, 12.0 mmol), and Pd $(PPh_3)_4$ (116.0 mg, 1.0 mol) were combined in a two-phase solution (60.0 mL) of toluene/water (5:1). The mixture was refluxed for 2 h, cooled to room temperature and extracted with CH_2Cl_2. The solvent was dried over anhydrous magnesium sulfate and removed under reduced pressure. The residue was chromatographed on a silica gel eluted with n-hexane/dichloromethane (1:1) to yield 1.89 g (56%) of TTPA (**4**), a brown solid. The characteristics were as follows: mp 143 °C; IR (KBr): 3466 (br s), 2929, 2863, and 2849 cm^{-1}; ^1H NMR ($CDCl_3$) δ: 6.93 - 7.56 (m, 11H, Ar), 4.86 (s, 2H, NH); ^{13}C NMR ($CDCl_3$): 159.7, 146.5, 139.2, 138.6, 136.5, 128.7, 127.9, 127.1, 126.6, 126.4, 126.0, 125.9, 125.1, 124.8, 121.0, and 119.3; Anal $C_{18}H_{13}NS_3$; MS (EI) *m/z* (%): 339 (M+, 100), 323 (33), 247 (44), 165 (30), 92 (36), and 83 (34).

Synthesis of 4-(([2,2':5',2''-terthiophen]-3'-yl) phenyl hydrazine (TPHyd) (compound (5))

An ice-cold solution of sodium nitrite (290.0 mg, 4.2 mmol, 1.05 equiv.) in water (3.0 mL) was added drop-wise to a solution of TTPA (1.35 g, 4.0 mmol, 1 equiv.) in ethanol (14.0 mL) and conc. HCl (14.0 mL) over a period of 10 min at 0 °C. The reaction mixture was stirred at 0 °C for 1 h, and a solution of Tin(II) chloride dihydrate (4.7 g, 20.8 mmol, 5.2 equiv.) in conc. HCl (4.0 mL) was added drop-wise. The resulting precipitate was suspended in 50.0 mL of water and decomposed with 60.0 mL of 1.0 M NaOH solution. The product was then extracted with ethyl acetate. The organic phase was dried over anhydrous magnesium sulfate and evaporated to give the final product, which was TPHyd (**5**) in the form of a yellow solid (1.17 g, 83%); the mp was 124 °C; IR (KBr): 3405 - 3509 (br s), 2954, 2922, and 2853 cm^{-1}; ^1H NMR ($CDCl_3$) δ: 6.93 - 7.56 (m, 11H, Ar), 5.15 (br s, 1H), 4.72 (br s, 2H, NH); ^{13}C NMR($CDCl_3$): 157.8, 149.6, 143.4, 138.9, 136.0, 128.9, 127.6, 127.1, 126.8, 126.3, 126.1, 125.8, 125.3, 124.7, 121.3, and 119.5; Anal $C_{18}H_{14}N_2S_3$; MS (EI) *m/z* (%): 354 (M+, 100), 338 (45), 323 (35), 271 (29), 195 (32), 164 (49), 107 (38), and 83 (38).

Preparation of the Electrocatalytic Channel Electrodes

The channel electrodes (area: 0.0078 cm^2) were washed with 0.1 M HCl, ethanol, and several times with distilled water. A 0.001% AuNP solution was prepared from 0.1 M PBS containing 10.0 mM $HAuCl_4$ and 10.0 mM trisodium citrate, to which 0.1 M sodium borohydride was added dropwise while slowly stirring (see detail in the Electronic Supplementary Information). The average size of the AuNPs was estimated by TEM to be 5.0 (± 1.5 nm, 82%). A self-assembled TBA monomer layer was formed on the AuNPs by mixing 1.0 mM TBA monomer dissolved in 1:1 of di(propylene glycol) methyl ether and tri(propylene glycol) methyl ether followed by AuNPs at a 1:1 ratio for 12 h at 4 °C. The TBA-AuNP-containing solutions were placed in the microchannel and electrochemically polymerized on the channel wall. A polymer nanoparticles film was formed on the channel wall by potential cycling from 0.0 to +1.4 V for two cycles at a scan rate of 100 mV s^{-1} in 0.1 M PBS (pH 7.0). After that, the channel electrodes were washed with water to remove the excess monomer mixture. As shown, the polyTBA-covered AuNP layer-coated electrode was immersed for 12 h in 0.1 M PBS (pH 7.0) containing 10.0 mM EDC/NHS to activate the carboxylic acid groups of the polymer nanoparticles layer as an electrode substrate and to thereby immobilize the enzymes. The EDC/NHS-treated channel surfaces were then washed with the buffer solution and subsequently incubated for 24 h in a PBS (pH 7.0) solution containing 4.0 mg mL^{-1} GOx or HRP at 4 °C. By following this procedure, the GOx and HRP were covalently bound through their amine groups to carboxylic groups on the polyTBA-covered AuNP layer through amide bond formation. Similarly, THyd- and TPHyd-AuNP solutions were used for electropolymerization, and they were used for the catalytic cathode reaction of H_2O_2.

Cell Operation

The channel electrodes were made of GOx as anodes and the HRP-immobilized conjugated polymer (polyTBA), polyTHyd-, and polyTPHyd-AuNP were used as cathodes operated on an open-circuit voltage. The MBFC employed 10.0 mM glucose as an anodic fuel and anode-produced H_2O_2 as a cathodic fuel. The substrates were injected at a rate of 1.0 mL min^{-1} into the corresponding compartment of the cell using a Twin Syringe Pump, model 33 (Harvard Apparatus, Inc. USA). The voltage and current generated by the channel electrodes were measured by applying an external variable load resistance and digital multi-meter. The performance of the cell was evaluated by *I-V* curves obtained at the open circuit voltage.

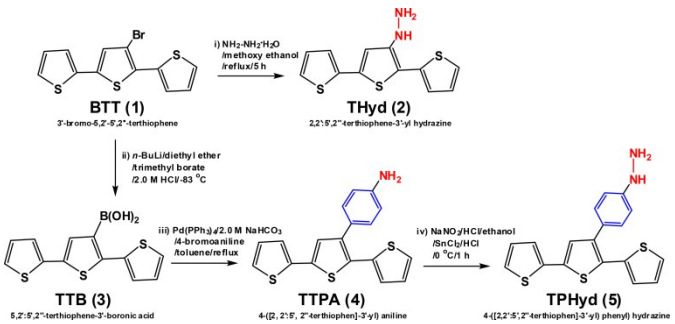

Scheme 1 Synthesis of THyd and TPHyd. Reagents and conditions: i) NH_2-NH_2·H_2O/methoxy ethanol/reflux/5 h, ii) *n*-BuLi/diethyl ether/trimethyl borate/2.0 M HCl/-83 °C, iii) $Pd(PPh_3)_4$/2.0 M $NaHCO_3$/4-bromoaniline/toluene/reflux, and iv) $NaNO_2$/HCl/ethanol/$SnCl_2$/HCl/0 °C/1 h.

Results and discussion

The 2,2′:5′,2′′-terthiophene-3′-yl hydrazine (THyd, ***2***) monomer was synthesized from BTT (***1***) *via* a one-step process. In this step, 3′-bromo-5,2′-5′,2′′-terthiophene (BTT) was refluxed with hydrazine hydrate in methoxy ethanol for a 67% yield of the desired THyd. A different monomer, called 4-(([2,2':5',2''-terthiophen]-3'-yl) phenyl hydrazine (TPHyd, ***5***), was also synthesized from BTT *via* a three-step process. In the first step, BTT was treated with *n*-BuLi and

trimethyl borate in Et_2O under a N_2 atmosphere at -83 °C to obtain 5,2′:5′,2″-terthiophene-3′-boronic acid (TTB, ***3***). The second step was the Suzuki coupling of the TTB with 4-bromoaniline in a refluxing two-phase solution of toluene/water (5:1) in the presence of $NaHCO_3$ and $Pd(PPh_3)_4$ to form 4-([2, 2':5', 2''-terthiophen]-3'-yl) aniline (TTPA, ***4***). In the third step, TTPA was treated with an ice-cold solution of sodium nitrite and a Tin(II) chloride dihydrate solution in ethanol/HCl to produce TPHyd at a yield of 83%. The final products (the monomers THyd and TPHyd (**Scheme 1**)) were characterized using spectroscopic methods (FT-IR, ^{1}H- and ^{13}C-NMR, and MS).

The MBFC was fabricated with the screen-printed microchannel electrode (SPME) as shown in **Scheme 2(A(a))**; the length of the channel electrode was 52.0 mm, the width of the flow channel was 100.0 ± 10.5 µm **Fig. S1(A)**, Electronic Supplementary Information, and the width of the carbon ink printed onto the microscope slide was 15.0 ± 2.5 µm, as shown in **Fig. S1(B)**, Electronic Supplementary Information. The detailed fabrication of microfluidic channel is explained in the Electronic Supplementary Information. In addition, a flexible type of microfluidic channel biofuel cell (FMBFC) was fabricated on polystyrene-based film using a similar method as previously described, as shown in **Scheme 2(A(b))**. All electrochemical and fuel cell experiments were performed using only the MBFC (**Scheme 2(A(a))**), not the FMBFC.

The immobilization steps of the biocatalysts (anode (*(i)* GOx/polyTBA-AuNPs) and cathodes (*(ii)* HRP/polyTBA-AuNPs, *(iii)* polyTHyd-AuNPs, and *(iv)* polyTPHyd-AuNPs) on the channel electrodes are shown in **Scheme 2(B)**. A layer of the polymer composite nanoparticles of the self-assembled TBA-, THyd-, and TPHyd-AuNP layers were formed on the channel wall by potential cycling from 0.0 to +1.4 V at a scan rate of 100 mV s^{-1} in 0.1 M phosphate buffer solution (PBS, pH 7.0). GOx and HRP were covalently bound to carboxylic groups of the polyTBA through the amide bond formation.

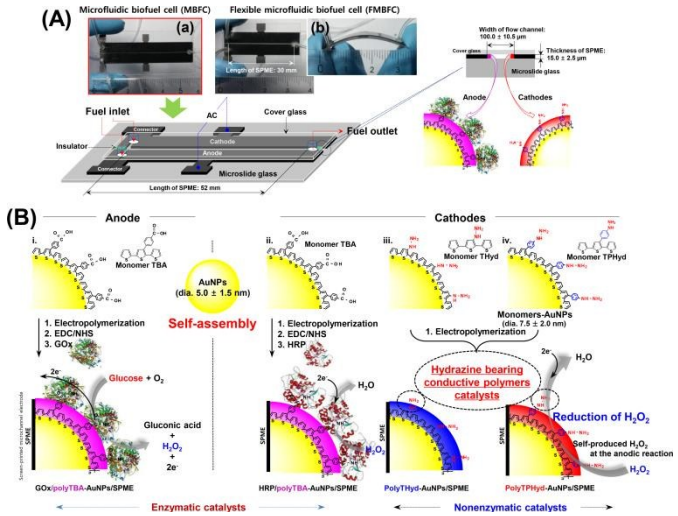

Scheme 2 (A) Schematic diagram of the experimental setup used to generate an AC potential in the (a) MBFC and (b) FMBFC. (B) Schematic preparation of the anode ((i) GOx/polyTBA-AuNPs) and cathodes ((ii) HRP/polyTBA-AuNPs, (iii) polyTHyd-AuNPs, and (iv) polyTPHyd-AuNPs).

The monomers were self-assembled on the AuNPs to create an extremely sensitive channel electrode surface through the formation of monomer-AuNP conjugates. These conjugates were characterized by UV-visible spectroscopy and TEM analysis. As shown in **Fig. 1(A)**, UV-visible spectra were obtained for **(a)** AuNPs, **(b)** TBA-, **(c)** THyd-, and **(d)** TPHyd-AuNPs in solution form. To obtain a self-assembled layer of monomer on the AuNPs with maximum surface coverage, the content ratio of the monomer to AuNPs was varied, and a 1:1 ratio was found to be optimal. The color of the AuNP solution differs before (pink at an absorption wavelength of 516.3 nm) and after (purple at absorption wavelengths 525.2, 525.8, and 525.9 nm) the formation of self-assembled TBA, THyd, and TPHyd layers on the AuNPs. **Fig. 1(B)** presents TEM images of **(a)** AuNPs, **(b)** TBA-, **(c)** THyd-, and **(d)** TPHyd-AuNPs solutions. In **Fig. 1(B(a))**, the size of the AuNPs was approximately 5.0 ± 1.5 nm. The thickness of the self-assembled monomer layer on the AuNPs was approximately 2.5 ± 0.5 nm. As shown in **Fig. 1(B(b-d))**, the self-assembled monomer on the AuNP formed sphere-shaped clusters of approximately 7.5 ± 2.0 nm in diameter. The inset in **Fig. 1(B)** shows corresponding size distributions of **(a)** AuNPs and **(b-d)** self-assembled monomer-AuNPs. The average size of the nanoparticles is nearly 5.0 ± 1.5 nm (82%) and that of monomer-AuNPs is 7.5 ± 2.0 nm (56 - 72%).

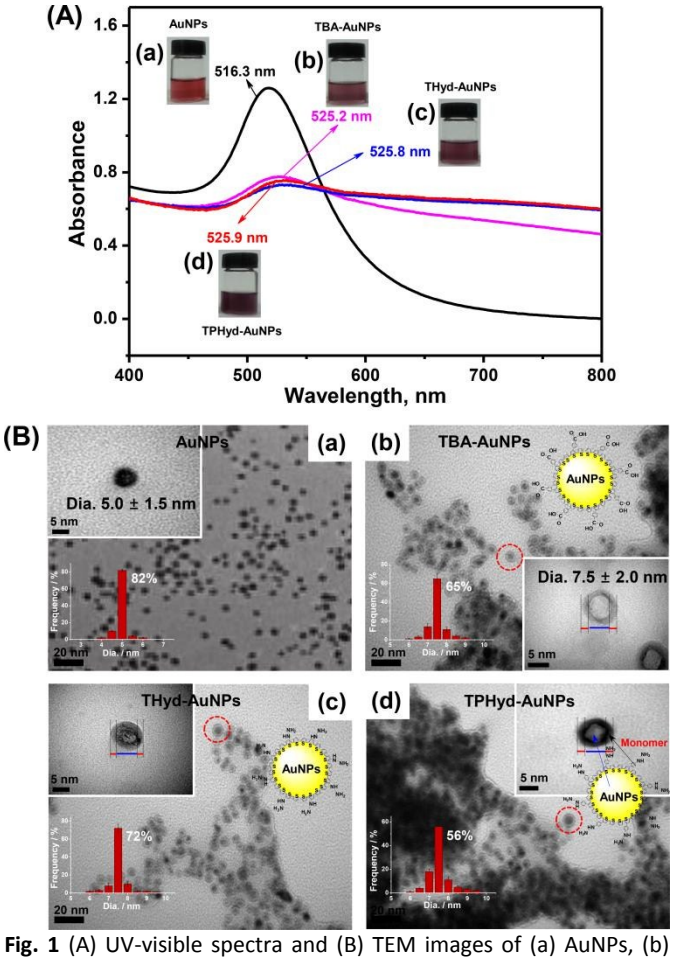

Fig. 1 (A) UV-visible spectra and (B) TEM images of (a) AuNPs, (b) TBA-, (c)THyd-, and (d) TPHyd-AuNPs solutions. Inset: High magnification images and size distribution of the nanoparticles.

The electropolymerization of a self-assembled monomer on AuNPs was performed on the microfluidic channel electrodes by cycling the potential between 0.0 and +1.4 V two times at a scan rate of 100 mV s^{-1}. As shown in **Fig. 2(A)**, an increase in the oxidation peak current of **(a)** TBA-, **(b)** THyd-, and **(c)** TPHyd-AuNPs during each potential cycle occurs at approximately +1140.0 mV due to monomer oxidation, and a set of redox peaks is observed at

approximately +930.5/+462.2 mV on the AuNPs. Following polymerization, the channel electrode surfaces were washed with distilled water to remove the excess monomers and AuNPs. To obtain polymer-AuNP layers with maximum surface coverage, the effect of the scan rate during the electropolymerization experiment was studied. The thickness of the polymer-AuNP layers after three cycles decreased with an increasing scan rate (between 50 and 200 mV s^{-1}), indicating the formation of a thin polymer layer at a higher scan rate. The polymer-AuNPs exhibited a large surface area, which provided an additional advantage for immobilization of a large amount of GOx and HRP onto the polymer-covered AuNP layer. Following the electropolymerization of the monomer-AuNP nanocomposite clusters on the channel electrode surface, a three-dimensional homogeneous compact structure was obtained, possessing good stability and preparation reproducibility. The compact nanocomposite film provided a significant increase in efficient active sites and yielded a good electrochemical response.

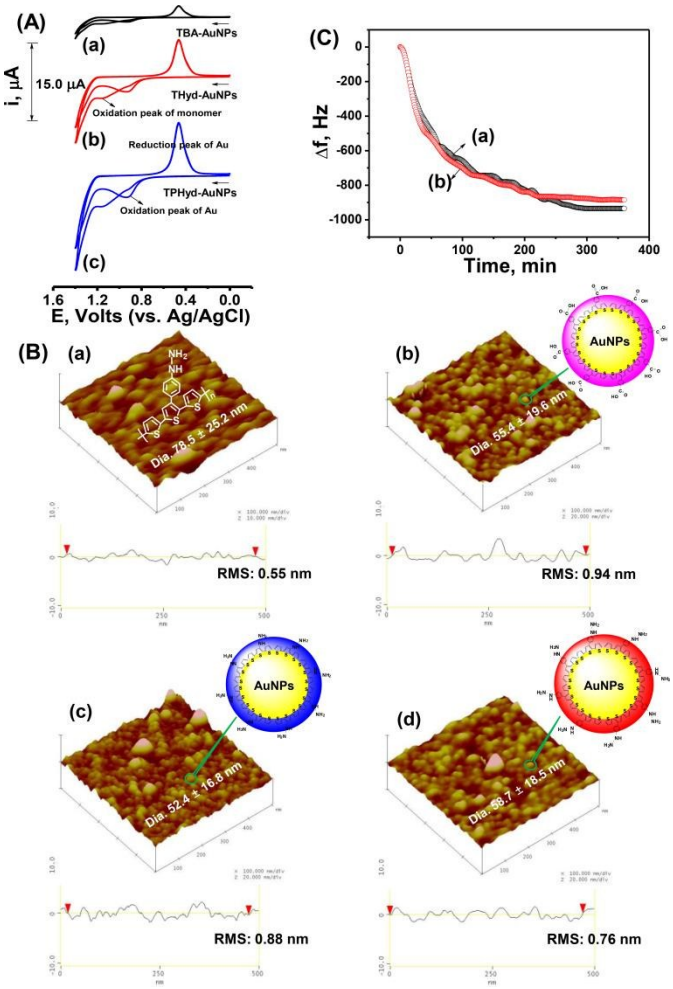

Fig. 2 (A) CVs recorded for the (a) TBA-, (b) THyd-, and (c) TPHyd-AuNP-containing solutions that were prepared in a 1:1 solution of di(propylene glycol) methyl ether and tri(propylene glycol) methyl ether; the solvent was dried and then transferred for electropolymerization. A polymer nanoparticles layer was formed in the SPME by potential cycling twice from 0.0 to +1.4 V at a scan rate of 100 mV s^{-1} in 0.1 M PBS (pH 7.0). (B) Tapping mode AFM images of the (a) polyTPHyd, (b) polyTBA-AuNPs, (c) polyTHyd-AuNPs, and (d) polyTPHyd-AuNP films; the image size is 500.0 nm × 500.0 nm. (C) Frequency changes during the immobilization of (a) GOx and (b) HRP onto polyTBA-AuNPs on a Au electrode.

The morphologies of the polymer films after electropolymerization were observed by AFM in tapping mode. The polyTPHyd, polyTBA-, polyTHyd-, and polyTPHyd-AuNP layers were formed through the electropolymerization of the monomer and self-assembled monomer-AuNPs coated on the highly oriented pyrolytic graphite (HOPG) electrode surface. The polymer nanoparticles coated on a HOPG electrode exhibits a homogeneous composition of small particles for the polymer-AuNP films. The particle sizes of **(a)** polyTPHyd, **(b)** polyTBA-, **(c)** polyTHyd-, and **(d)** polyTPHyd-AuNPs films were determined to be 78.5 ± 25.2, 55.4 ± 19.6, 52.4 ± 16.8, and 58.7 ± 18.5 nm, respectively (**Fig. 2(B)**). The differences in the root-mean-square roughness of the surfaces among the polyTPHyd, polyTBA-, polyTHyd, and polyTPHyd-AuNPs films (0.55, 0.94, 0.88, and 0.76 nm, respectively) are small, as shown in **Fig. 2(B)**. QCM experiments were also performed to determine the amounts of **(a)** GOx and **(b)** HRP immobilized on the polymer-AuNP film (**Fig. 2(C)**). Frequency changes were observed as GOx and HRP were immobilized on the polyTBA layer through amide bond formation with activated carboxylic acid groups. The decrease in frequency reached a steady state after 300 and 220 min, with overall frequency changes (Δf) of 934.9 and 864.1 kHz, respectively. The immobilized amounts of GOx and HRP were determined to be 1027.8 ng (3.4×10^{-11} mol cm^{-2}) and 950.1 ng (1.2×10^{-10} mol cm^{-2}) according to a previously defined equation.[19] These results confirm that GOx and HRP are successfully immobilized onto the polymer nanoparticles layer.

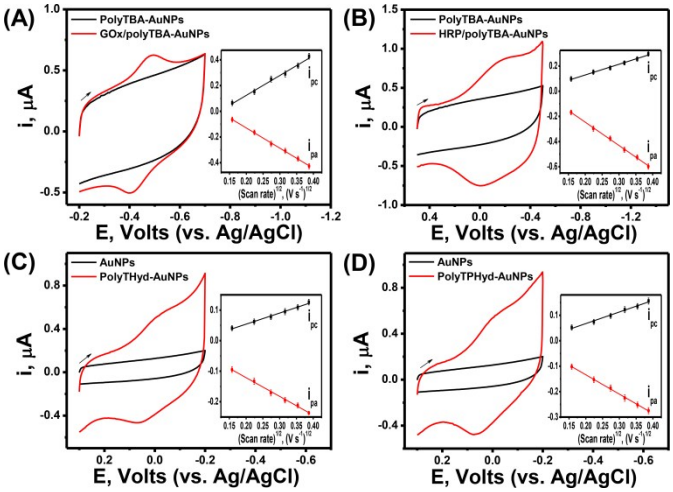

Fig. 3 CVs for the DET of the (A) GOx, (B) HRP, (C) polyTHyd, and (D) polyTPHyd modified electrodes in 0.1 M PBS (pH 7.0) at a scan rate of 50 mV s^{-1}. Inset: Plot of i_{pc} *versus* $v^{1/2}$ and i_{pa} *versus* $v^{1/2}$ from voltammograms ($n = 3$). Scan rate (v): 25, 50, 75, 100, 125, and 150 mV s^{-1}.

The final modified electrode surface reveals the DET processes of GOx and HRP, in addition to the enzyme-like polyTHyd and polyTPHyd, which were observed first. **Fig. 3** shows the redox peaks generated by DET for **(A)** GOx and **(B)** HRP immobilized on the conducting polymer (polyTBA-AuNPs) and **(C)** polyTHyd-AuNPs and **(D)** polyTHyd-AuNP-modified electrodes in 0.1 M PBS (pH 7.0) at a scan rate of 50 mV s^{-1}. The formal potentials ($^{o}E'$) were -444.6 mV for GOx, -87.7 mV for HRP, +16.8 mV for polyTHyd, and +34.2 mV for polyTPHyd (*vs.* Ag/AgCl). In this case, the favored orientation of enzyme molecules and the conducting channels of the polymer electrode resulted in DET processes[37,38] between the prosthetic groups of the enzymes and the conducting polymer nanoparticles-

coated electrode surfaces. The ratio of cathodic to anodic peak currents is nearly unity. Peak currents vary linearly with the scan rate, as shown in the inset of **Fig. 3**, indicating that the electrode process is not diffusion controlled, as expected for an immobilized and polymerized system. The cathodic and anodic peak potentials shift very slightly in opposite directions with a change in the scan rate. The separation between the peak potential (ΔE_p) is 70.4, 140.1, 75.4, and 61.2 mV at a scan rate of 50 mV s^{-1}. We calculated the electron transfer rate constant (k_s) as 0.49, 0.25, 0.47, and 0.54 s^{-1} for GOx, HRP, polyTHyd, and polyTPHyd, respectively, using the data for 50 mV s^{-1} from **Fig. 3** by adopting a previously reported method.[39] This result indicates that enzyme-mimicking hydrazine-bearing polymers nanoparticles (polyTHyd and polyTPHyd) exhibit enhanced electron transfer compared with the enzymatic biomaterials, of which polyTPHyd exhibits the best electron transfer due to the π-π^* transition of the benzyl group. Therefore, this pair of peaks originates from the redox reaction of the electroactive sites of GOx and HRP on the conducting polymer-modified electrode and hydrazine-bearing polymer nanoparticles. Considering the fact that HRP, polyTHyd, and polyTPHyd alone do not exhibit observable peaks at the SPME surface, the electron transfer process is considerably enhanced by the conducting polymer nanoparticles.

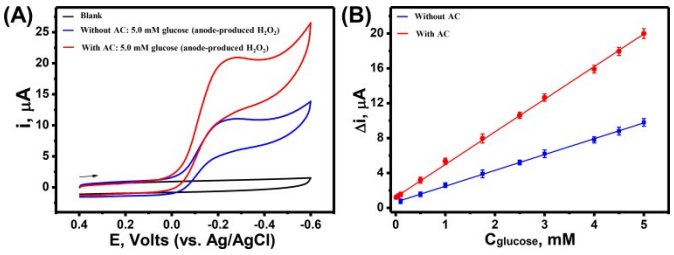

Fig. 4 (A) CVs recorded for GOx/polyTBA-AuNPs and polyTPHyd-AuNPs in 0.1 M PBS (pH 7.0, black line) and in a PBS containing 0.1 - 5.0 and 0.01 - 5.0 mM glucose (anode-produced H_2O_2) under the conditions without (blue line) and with AC (red line) potential application at a scan rate of 50 mV s^{-1}. (B) Calibration plot for different concentrations of glucose.

The DET process of GOx electrode will be utilized as an analytical tool to detect glucose as a third generation type biosensors. To confirm H_2O_2 generation through an enzymatic reaction in a first generation type, we investigated whether H_2O_2 produced from GOx/polyTBA-AuNPs/SPME was efficiently reduced by the polyTPHyd-AuNP-modified electrode. **Fig. 4(A)** shows the CVs recorded between +0.4 and -0.6 V for the polyTPHyd-AuNP-modified electrode in 0.1 M PBS (pH 7.0) using blank PBS (black line) and a glucose solution without AC (blue line) and with AC (red line) at a scan rate of 50 mV s^{-1}. No catalytic current was observed in a blank electrolyte solution due to the absence of glucose; however, a H_2O_2 reduction peak was clearly observed at -0.23 V in a 5.0 mM glucose solution. This result indicates that the GOx/polyTBA-AuNPs/SPME generated H_2O_2 through an enzymatic reaction and that the polyTPHyd-AuNP electrode catalytically reduced H_2O_2. The calibration plots with and without AC potential application were obtained: The dynamic range with AC was determined to be between 10.0 μM and 5.0 mM (red line), and one without AC was between 100.0 μM and 5.0 mM (blue line) (Fig. 4(B)). The linear regression equations were respectively expressed as follows: ΔIp (μA) = 1.22 (± 0.12) + 3.74 (± 0.06) [glucose (anode-produced H_2O_2) mM] with a correlation coefficient of 0.999 (with AC), and ΔIp (μA) = 0.66 (± 0.17) + 1.81 (± 0.07) [glucose (anode-produced H_2O_2) mM] with a correlation coefficient of 0.999 (without AC). The detection limit for glucose (anode-produced H_2O_2) was determined to be 2.5 ± 0.2 μM (RSD < 5%) based on the standard deviation for the three times measurement in the blank solution (95% confidence level, $k = 3$, $n = 3$).

Fig. 5(A) presents a schematic for an MBFC anode (GOx) and cathodes (HRP-, polyTHyd-, or polyTPHyd-) in a glucose-containing buffer solution. The enzyme and artificial enzyme-catalyzed reactions are illustrated in the following scheme:

$$\text{Anodic: Glucose} + O_2 \xrightarrow{\text{GOx}} \text{Gluconic acid} + H_2O_2 + 2e^- \quad (1)$$

$$\text{Cathodic: } H_2O_2 + 2e^- + 2H^+ \xrightarrow{\text{HRP,polyTHyd,or polyTPHyd}} H_2O \quad (2)$$

The biocatalytic reactions involve the oxidation of glucose by GOx and the reduction of H_2O_2 produced in the anodic enzyme reaction by HRP, polyTHyd, or polyTPHyd on the channel electrode surface. The electrons are shuttled between the enzyme and conducting polymer nanoparticles-modified electrode substrates. In this case, the cell performance was evaluated using 10.0 mM glucose ($n=3$). **Fig. 5(B)** shows *I-V* and *I-P* curves plotted with GOx/polyTBA-AuNPs/SPME as an anode and (*Com. 1*) HRP/polyTBA-AuNPs, (*Com. 2*) polyTHyd-AuNPs, and (*Com. 3*) polyTPHyd-AuNPs/SPME as cathodes **(a)** without an AC potential application on the channel electrodes. These compositions provide 0.02 ± 0.001, 0.05 ± 0.002, and 0.58 ± 0.019 mW cm^{-2} of power density, 0.39 ± 0.018, 0.44 ± 0.027, and 0.47 ± 0.031 V of cell voltage, and 0.11 ± 0.005, 0.20 ± 0.011, and 1.95 ± 0.095 mA cm^{-2} of current density, respectively. As shown in **(b)** with the application of an AC potential, (*Com. 4*) GOx/polyTBA-AuNPs/SPME as the anode and polyTPHyd-AuNPs/SPME as the cathode provides 0.78 ± 0.034 mW cm^{-2} of power density, as calculated from 0.48 ± 0.035 mV of cell voltage and 2.65 ± 0.126 mA·cm^{-2} of current density. The power density is 1.4-fold higher with the AC potential than without. These results reveal that the combination of GOx/polyTBA-AuNPs and polyTPHyd-AuNPs provides the highest power density for the MBFCs (**Table 1**).

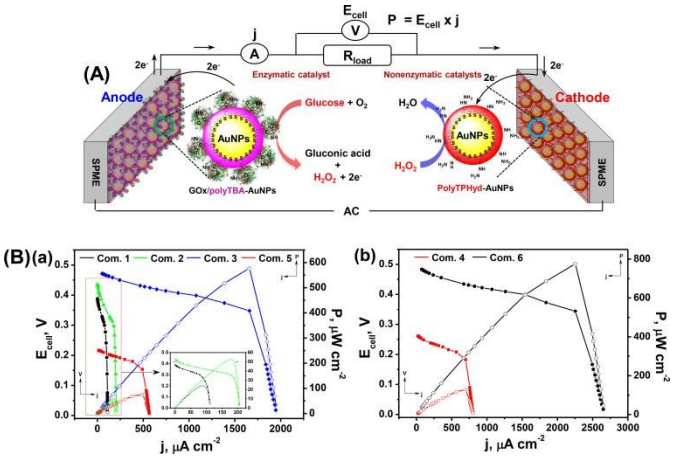

Fig. 5 (A) Schematic diagram of a MBFC. (B) *I-V* and *I-P* curves for glucose and human whole blood as anode fuels (anode-produced H_2O_2) generated by GOx/polyTBA-AuNPs (anode) and HRP/polyTBA-AuNP, polyTHyd-AuNP, or polyTPHyd-AuNP (cathodes) electrodes (a) without and (b) with AC potential application.

The power density of the present study is 8.2-fold higher than that previously reported for the same enzyme composition.[40] In this case, the higher power density is achieved by shortening the distance between the enzyme redox center and electrode surface[41,42] and enhancing the catalytic action of the artificial enzymes, polyTHyd-AuNPs and polyTPHyd-AuNPs. Most of

studies[43,44] have employed O_2 as a cathodic fuel, whereas our system uses the H_2O_2 produced at the anode. In addition to glucose, human whole blood (a blood glucose level of 98.5 mg dL^{-1}) can be used as the anodic fuel, indicating that this instrument can be used to monitor the glucose level in blood. In this case, the cell performance at 25 °C exhibited the following characteristics: cell voltages of 0.22 ± 0.007 and 0.26 ± 0.080 V, current densities of 0.57 ± 0.035 and 0.80 ± 0.048 mA cm^{-2}, and power densities of (*Com. 5*) 0.08 ± 0.003 and (*Com. 6*) 0.13 ± 0.005 mW cm^{-2}. The cell operated with a 10.0 mM glucose solution generated a maximum electrical power density of 0.78 ± 0.034 mW cm^{-2} and an open-circuit voltage of 0.48 ± 0.035 V. However, normal urine sample contains negligible concentration of glucose, which revealed very low (~0.001 ± 0.001 mW cm^{-2} of power density). MBFCs composed of several conducting polymer nanoparticles-coated electrode combinations have been examined to evaluate the cell performance, as summarized in **Table 1**. The effect of O_2 on the cell performance was also examined. The biofuel cell working in the absence of oxygen gas in the channel yields a low cell voltage of 0.36 ± 0.015 V, the current density of 0.62 ± 0.038 mA cm^{-2}, and the power density of 0.16 ± 0.008 mW cm^{-2}. Control experiments without glucose and GOx show immeasurably low values. However, only GOx attachment without self-assembling on AuNPs showed a decreased density as the follows; 0.42 ± 0.025 V of cell voltage, 0.85 ± 0.052 mA cm^{-2} of current density, and 0.18 ± 0.009 mW cm^{-2} of power density (see **Table S1**, Electronic Supplementary Information). The cell performance was compared with other enzyme systems (see **Table S2**, Electronic Supplementary Information).

Table 1. Performance of the MBFCs (*n=3*).

Samples	Com. of the MBFCs	Anodic Fuels	Anodes	Cathodes	Cell voltage, E (V)	Current density, j (mA cm^{-2})	Power density, P (mW cm^{-2})
Standard	Com. 1.	Glucose and O_2	GOx/polyTBA-AuNPs	HRP/polyTBA-AuNPs	0.39 (± 0.018)	0.11 (± 0.005)	0.02 (± 0.001)
	Com. 2.			PolyTHyd-AuNPs	0.44 (± 0.027)	0.20 (± 0.011)	0.05 (± 0.002)
	Com. 3.			PolyTPHyd-AuNPs	0.47 (± 0.031)	1.95 (± 0.095)	0.58 (± 0.019)
	Com. 4.			PolyTPHyd-AuNPs *(with AC potential)*	0.48 (± 0.035)	2.65 (± 0.126)	0.78 (± 0.034)
Real	Com. 5.	Human whole blood and O_2		PolyTPHyd-AuNPs	0.22 (± 0.007)	0.57 (± 0.035)	0.08 (± 0.003)
	Com. 6.			PolyTPHyd-AuNPs *(with AC potential)*	0.26 (± 0.080)	0.80 (± 0.048)	0.13 (± 0.005)
	Not shown	Urine and O_2			~0.003 (± 0.001)	~0.007 (± 0.002)	~0.001 (± 0.001)

Alternating current (AC) potential: 1.0 V, 1.0 MHz; Flow rate of fuel: 1.0 mL min^{-1}; Electrode area: 0.0078 cm^2

To evaluate the long-term stability of the cell, the current density of the cell using 10.0 mM glucose was continuously recorded for 16 days. The cell delivered 2.08 ± 0.098 mA cm^{-2} after 16 days, which represented 78% of its initial performance, and it showed the long lifetime for a cathode using enzymes. The power density in an enzyme-based MBFC is closely related to the enzyme activity, and enzyme inactivation would result in a decrease in the power density. However, the lifetime of the present MBFC composed of the conducting polymer nanoparticles was 16 days, showing ~1.6 and ~3.2-fold higher than that of previously reported biofuel cells composing of GOx and laccase modified electrodes,[45] and glucose dehydrogenase and polydimethylsiloxane/Pt modified electrodes in a microfluidic channel.[46] This might be that enzymes were immobilized on the electrodes surface by chemical bonding.

Conclusions

Functionalized conducting polymer nanoparticles (polyTHyd and polyTPHyd) formed on self-assembled AuNPs were successfully demonstrated to glucose MBFCs as enzyme-like catalysts. The attained DET process was used for the BFC and biosensor device. The catalytic activity of the cathode was largely improved by introducing polyTHyd- and polyTHyd-assembled nanoparticles on the channel electrode. Electricity was successfully generated through the construction of the MBFC, and the maximum power density was 0.78 mW cm^{-2} at the external optimal load of 25.0 kΩ. The lifespans of the MBFC when using these conjugated polymer-assembled nanoparticles were over five months. Hence, the power density and lifetime of the proposed MBFCs were improved using polyTHyd- and polyTPHyd-assembled AuNPs by overcoming the limitations of enzyme-based MBFCs. Furthermore, the BFC sensor exhibited dynamic ranges of 10.0 μM - 5.0 mM with a detection limit of 2.5 ± 0.2 μM. The MBFC fabricated in this study exhibits a wide range of potential applications for various energy convertors and bio-/chemical sensors as well as implantable bio-devices.

Acknowledgements

This work was supported by the Program through NRF grant funded by the MEST (Grant 2015R1A2A1A13027762).

Notes and references

1 S. P. Jiang and P. K. Shen, in *Nanostructured and Advanced Materials for Fuel Cells*, CRC Press, New York, 2013.
2 M. C. Potter, *Proc. R. Soc. Lond. B*, 1911, **84**, 260.
3 R. A. Bullen, T. C. Arnot, J. B. Lakeman and F. C. Walsh, *Biosens. Bioelectron.*, 2006, **21**, 2015.
4 S. K. Chaudhuri and D. R. Lovley, *Nat. Biotechnol.*, 2003, **21**, 1229.
5 S. C. Barton, J. Gallaway and P. Atanassov, *Chem. Rev.*, 2004, **104**, 4867.
6 E. Katz and K. MacVittie, *Energy Environ. Sci.*, 2013, **6**, 2791.
7 T. Miyake, K. Haneda, N. Nagai, Y. Yatagawa, H. Onami, S. Yoshino, T. Abec and M. Nishizawa, *Energy Environ. Sci.*, 2011, **4**, 5008.
8 S. Vaddiraju, I. Tomazos, D. J. Burgess, F. C. Jain and F. Papadimitrakopoulos, *Biosens. Bioelectron.*, 2010, **25**, 1553.
9 B. Yu, N. Long, Y. Moussy and F. A Moussy, *Biosens. Bioelectron.*, 2006, **21**, 2275.
10 L. Halamkova, J. Halamek, V. Bocharova, A. Szczupak, L. Alfonta and E. Katz, *J. Am. Chem. Soc.*, 2012, **134**, 5040.
11 M. Grzelczak, J. Vermant, E. M. Furst and L. M. Liz-Marzán, *ACS Nano*, 2010, **4**, 3591.
12 O. Yehezkeli, R. Tel-Vered, S. Raichlin and I. Willner, *ACS Nano*, 2011, **5**, 2385.
13 K. Murata, K. Kajiya, N. Nakamura and H. Ohno, *Energy Environ. Sci.*, 2009, **2**, 1280.
14 Y. Chen, P. Gai, J. Zhang and J. -J. Zhu, *J. Mater. Chem. A*, 2015, **3**, 11511.
15 N. Mano, H. -H. Kim, Y. Zhang and A. Heller, *J. Am. Chem. Soc.*, 2002, **124**, 6480.
16 N. Mano, F. Mao and A. Heller, *J. Am. Chem. Soc.*, 2003, **125**, 6588.

17 M. Gerard, A. Chaubey and B. D. Malhotra, *Biosens. Bioelectron.*, 2002, **17**, 345.
18 A. K. Sarma, P. Vatsyayan, P. Goswami and S. D. Minteer, *Biosens. Bioelectron.*, 2009, **24**, 2313.
19 H. -B. Noh, P. Chandra, J. O. Moon and Y. -B. Shim, *Biomaterials*, 2012, **33**, 2600.
20 J. Wang, *Chem. Rev.*, 2008, **108**, 814.
21 H. -B. Noh, M. -S. Won, J. Hwang, N. -H. Kwon, S. C. Shin and Y. -B. Shim, *Biosens. Bioelectron.*, 2010, **25**, 1735.
22 S. Xu and S. D. Minteer, *ACS Catal.*, 2014, **4**, 2241.
23 G. Inzelt, in *Conducting Polymers: A New Era in Electrochemistry*, Springer-Verlag, Heidelberg, 2012.
24 M. J. Cooney, V. Svoboda, C. Lau, G. Martina and S. D. Minteer, *Energy Environ. Sci.*, 2008, **1**, 320.
25 H. J. Salavagione, A. M. Diez-Pascual, E. Lazaro, S. Vera and M. A. Gomez-Fatoua, *J. Mater. Chem. A*, 2014, **2**, 14289.
26 T. S. Zhao, in *Micro Fuel Cells: Principle and Applications*, Elsevier, Burlington, 2009.
27 A. Kundu, J. H. Jang, J. H. Gil, C. R. Jung, H. R. Lee, S. -H. Kim, B. Ku and Y. S. Oh, *J. Power Sources*, 2007, **70**, 67.
28 E. Kjeang, N. Djilali and D. Sinton, *J. Power Sources*, 2009, **186**, 353.
29 C. M. Moore, S. D. Minteer and R. S. Martin, *Lab Chip*, 2005, **5**, 218.
30 M. A. dos Santos Bernardes, in *Enzyme-Based Microfluidic Biofuel Cell to Generate Micropower*, ed. A. Zebda, C. Innocent, L. Renaud, M. Cretin, F. Pichot, R. Ferrigno and S. Tingry, InTech, 2011.
31 A. Zebdaa, L. Renaudb, M. Cretina, C. Innocenta, R. Ferrignob and S. Tingrya, *Sens. Actuator B-Chem.*, 2010, **149**, 44.
32 A. Zebda, L. Renaud, M. Cretin, F. Pichot, C. Innocent, R. Ferrigno and S. Tingry, *Electrochem. Commun.*, 2009, **11**, 592.
33 R. S. Jayashree, L. Gancs, E. R. Choban, A. Primak, D. Natarajan, L. J. Markoski and P. J. A. Kenis, *J. Am. Chem. Soc.*, 2005, **127**, 16758.
34 E. R. Choban, L. J. Markoski, A. Wieckowski and P. J. A. Kenis, *J. Power Sources*, 2004, **128**, 54.
35 S. M. H. Hashemi, M. A. Modestino and D. Psaltis, *Energy Environ. Sci.*, 2015, **8**, 2003.
36 D. -M. Kim, J. -H. Yoon, M. -S. Won and Y. -B. Shim, *Electrochim. Acta*, 2012, **67**, 201.
37 Md. A. Rahman, M. -S. Won and Y. -B. Shim, *Biosens. Bioelectron.*, 2005, **21**, 257.
38 Y. -T. Kong, M. Boopathi and Y. -B. Shim, *Biosens. Bioelectron.*, 2003, **19**, 227.
39 E. Laviron, *J. Electroanal. Chem.*, 1979, **101**, 19.
40 A. Trifonov, K. Herkendell, R. Tel-Vered, O. Yehezkeli, M. Woerner and I. Willner, *ACS Nano*, 2013, **7**, 11358.
41 A. Pizzariello, M. Stredansky and S. Miertus, *Bioelectrochemistry*, 2002, **56**, 99.
42 W. Vielstich, H. Gasteiger and A. Lamm, in *Handbook of Fuel Cells-Fundamentals, Technology, Applications*, Wiley, New York, 2003, vol. 4, pp. 355-381.
43 N. Mano and A. Heller, *J. Electrochem. Soc.*, 2003, **150**, A1136.
44 V. Soukharev, N. Mano and A. Heller, *J. Am. Chem. Soc.*, 2004, **12**, 8368.
45 M. G. Bellino and G. J. A. A. Soler-Illia, *Small*, 2014, **10**, 2834.
46 M. Togo, A. Takamura, T. Asai, H. Kaji and M. Nishizawa, *Electrochim. Acta*, 2007, **52**, 4669.

Table of contents entry

Hydrazine-bearing terthiophenes were self-assembled and polymerized on AuNPs to yield enzyme-like catalytic activity for the H_2O_2 reduction in a MBFC.